



A polarization model for a solid oxide fuel cell with a mixed ionic and electronic conductor as electrolyte

Shuanglin Shen ^a, Yupeng Yang ^a, Liejin Guo ^{a,1}, Hongtan Liu ^{b,*}

^a International Research Center for Renewable Energy, State Key Laboratory of Multiphase Flow in Power Engineering, Xi'an Jiaotong University, Xi'an, Shaanxi 710049, China

^b Clean Energy Research Institute, Department of Mechanical and Aerospace Engineering, University of Miami, Coral Gables, FL 33124, USA



HIGHLIGHTS

- SOFC model with a mixed ionic–electronic conductor electrolyte is developed.
- The modeling results agree well with experimental data.
- Effects of various parameters are studied.
- The distribution of oxygen partial pressure in the MIEC electrolyte is obtained.

ARTICLE INFO

Article history:

Received 17 October 2013

Received in revised form

6 January 2014

Accepted 8 January 2014

Available online 16 January 2014

Keywords:

Polarization model

Solid oxide fuel cell

Mixed ionic and electronic conductor

Leakage current

ABSTRACT

A polarization model for a solid oxide fuel cell (SOFC) with a mixed ionic and electronic conductor (MIEC) electrolyte is developed based on charge transport equation and a constant ionic conductivity assumption. The electrochemical reaction at the electrode is described by the Butler–Volmer equation and the energy conservation equation is included as an additional condition to complete the model. The modeling results agree well with experimental data. Utilizing this model the effects of key parameters, including conductivities of electrolyte, electrolyte thickness and cathode exchange current density on the performance of the SOFC are analyzed. The distribution of oxygen partial pressure in the electrolyte is also obtained.

© 2014 Elsevier B.V. All rights reserved.

1. Introduction

Acceptor doped ceria (ADC) is a promising candidate electrolyte material for solid oxide fuel cells (SOFC) since it allows the SOFC to operate at intermediate temperature (500–800 °C) [1–4] thanks to its high ionic conductivity in such temperature range. However acceptor doped ceria is a mixed ionic and electronic conductor (MIEC) at the typical SOFC operating conditions and has considerable electronic conductivity at low oxygen partial pressure due to the partial reduction of Ce⁴⁺ to Ce³⁺ [5], resulting in significantly lower open-circuit potential [6,7].

Mathematical models are important in analyzing and studying the complex phenomena in fuel cells and are also useful tools for fuel cell design and operations. There are many modeling studies

on the SOFC with pure ionic conducting electrolyte (e.g. YSZ) [8–12], but only limited modeling studies [13–20] are reported for SOFCs with a MIEC electrolyte. Choudhury and Patterson [20] obtained expressions for the current and voltage of a SOFC with a MIEC electrolyte using the Wagner's theory, and with these expressions, *I*–*V* relationship of the SOFC with a MIEC electrolyte can be obtained. Tannhauser [19] developed a model for a SOFC with a MIEC electrolyte based on the charge transport equation and the electric neutrality assumption, and obtained the *I*–*V* relationship and open-circuit voltages. Riess [18] developed a model based on the charge transport equation and the assumption of constant ionic conductivity, and an explicit expression of electronic current was obtained. However all of the above models were based on reversible electrode and the electrode reaction kinetics were not taken into consideration.

Riess, Gödickemeier and Gauckler [16,17] developed an electrode reaction model for a SOFC with a MIEC electrolyte. In the model the overpotentials at both electrodes were separated into

* Corresponding author. Tel.: +1 3052842019; fax: +1 3052842580.

E-mail addresses: lj-guo@mail.xjtu.edu.cn (L. Guo), hliu@miami.edu (H. Liu).

¹ Tel.: +86 29 8266 3895; fax: +86 29 8266 9033.

three parts, i.e. mass diffusion loss, charge transfer loss and chemical reaction loss. However several parameters were used in the expressions of the overpotential and these parameters were obtained by fitting the modeling results with experiment data. Wachsman et al. [13,15] developed a continuum-level analytical model for a SOFC with a MIEC electrolyte according to the transport equation and the charge neutrality assumption. The electrode reactions were described by combining the Butler–Volmer equation and the defect equilibrium equation. In this model, only one parameter K (the equilibrium constant) need to be calculated by comparing numerical results with experimental data.

In this work a polarization model of a SOFC with a MIEC electrolyte is developed according to the transport equation and the constant ionic conductivity assumption, and the electrochemical reaction at the electrode is described by the Butler–Volmer equation. The energy conservation equation as a supplementary equation is first introduced to complete the model. No model parameters need to be obtained by fitting experiment data. Thus this model is more rigorous than the existing models and has wider applications. The modeling results are compared with experimental data and the effects of some key parameters on the performance of SOFC with a MIEC electrolyte are studied.

2. Model development

A 1D configuration of a SOFC with a MIEC electrolyte is considered and the charge transport is shown in Fig. 1. In this model oxygen ions and electrons are the only mobile charges, and the electrochemical reaction is assumed to occur only in the interface between electrodes and electrolyte. The current direction from the anode to cathode is defined as positive, thus the ionic current is positive and electronic current is negative. This opposite direction is due to the different driving force for ions and electrons. The potential at the anode is specified to be zero and that at the cathode is specified to be the cell voltage, V .

2.1. Charge transport in a MIEC

The fundamental equations of the model are the charge transport equation (Nernst–Planck equation) and the continuity equation at steady state,

$$J_i(x) = -D_i \frac{\partial c_i(x)}{\partial x} - \frac{\sigma_i(x) \partial \phi(x)}{z_i e} \quad (1)$$

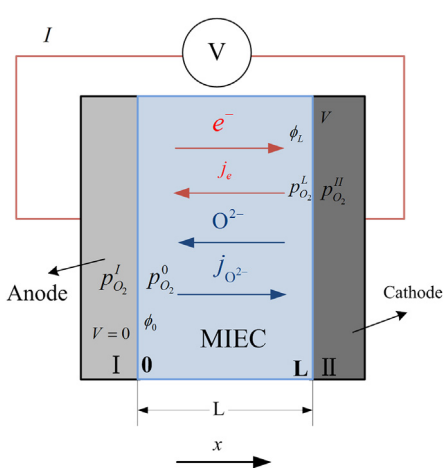


Fig. 1. The schematic of the charge transport in the SOFC with a MIEC electrolyte.

$$\frac{\partial}{\partial x} J_i(x) = 0 \quad (2)$$

where $J_i(x)$ is the mole flux of charge i , D is the diffusivity, c is the charge concentration, σ is the conductivity, z_i is the charge number and ϕ is the static potential. As in some existing studies [21–23], the assumption of constant ionic conductivity is used, thus the concentration of oxygen ions is constant in the electrolyte,

$$\frac{\partial c_{O^{2-}}}{\partial x} = 0. \quad (3)$$

Then the ionic current density is obtained from Eqs. (1) and (3) as:

$$j_{O^{2-}} = -\sigma_{O^{2-}} \frac{\partial \phi}{\partial x} \quad (4)$$

Since the electronic conductivity of a MIEC obeys the $-1/n$ power of the oxygen partial pressure p_{O_2} [24], and n is assumed to be 4 for acceptor doped ceria, thus:

$$\sigma_e = \sigma_e^0 p_{O_2}^{-1/4} \quad (5)$$

where σ_e^0 is a temperature-dependent coefficient that is independent of oxygen partial pressure. The relationship between the ionic and electronic current densities is obtained by an early theoretical model [25] as:

$$\frac{j_{O^{2-}}}{\sigma_{O^{2-}}} - \frac{j_e}{\sigma_e} = \frac{RT}{4F} \frac{\partial(\ln p_{O_2})}{\partial x}. \quad (6)$$

where R is the gas constant, T is the absolute temperature and F is the Faraday constant.

Integrating Eq. (6) and the relationship between the ionic and electronic current densities can be obtained as:

$$j_e = \frac{j_{O^{2-}}}{\sigma_{O^{2-}} M_0 - 1} \left[M_0 (p_{O_2}^0)^{-1/4} - (p_{O_2}^L)^{-1/4} \right]. \quad (7)$$

where $p_{O_2}^0$ and $p_{O_2}^L$ are the oxygen partial pressures in the electrolyte at $x = 0$ and $x = L$, respectively, and

$$M_0 = \exp \left[-\frac{F}{RT} \frac{j_{O^{2-}} L}{\sigma_{O^{2-}}} \right]$$

By defining equivalent electronic conductivity $\hat{\sigma}_e$ as,

$$\hat{\sigma}_e = \frac{\sigma_e^0}{M_0 - 1} \left[M_0 (p_{O_2}^0)^{-1/4} - (p_{O_2}^L)^{-1/4} \right]$$

and substituting Eq. (4) into Eq. (7), the electronic current density can be expressed as:

$$j_e = -\hat{\sigma}_e \frac{\partial \phi}{\partial x} \quad (8)$$

From Eq. (6), the distribution of the oxygen partial pressure in the electrolyte can be obtained as [25],

$$[p_{O_2}(x)]^{-1/4} = \left[(p_{O_2}^0)^{-1/4} - A_0 \right] \exp \left(-\frac{F}{RT} \frac{j_{O^{2-}}}{\sigma_{O^{2-}}} x \right) + A_0 \quad (9)$$

where

$$A_0 = \frac{j_e}{j_{O^{2-}}} \frac{\sigma_{O^{2-}}}{\sigma_e^0}$$

2.2. The electrochemical reaction in the electrodes

The electrochemical reaction in the cathode is described by the Butler–Volmer equation,

$$j_{O^{2-}} = j_{0-c} \left\{ \exp \left(\alpha_c \frac{nF}{RT} \eta_c \right) - \exp \left[- (1 - \alpha_c) \frac{nF}{RT} \eta_c \right] \right\} \cdot \frac{p_{O_2}^{ll}}{p_{O_2}^{ref}} \quad (10)$$

where j_{0-c} is the exchange current density for the cathode, α_c is the cathode transfer coefficient ($\alpha_c = 0.5$), η_c is the activation polarization at the cathode, $p_{O_2}^{ll}$ is the oxygen partial pressure in the cathode and $p_{O_2}^{ref}$ is the reference oxygen partial pressure. The activation polarization is defined as:

$$\eta_c = V_{rev,c} - (V - \phi_L) \quad (11)$$

where $V_{rev,c}$ is the theoretical reversible voltage of the cathode, and ϕ_L is the static potential at $x = L$.

The electrochemical reaction in the anode is assumed to be reversible since the activation polarization in the anode is much smaller than that in the cathode at the intermediate temperature. Thus,

$$\eta_{an} = 0, \quad p_{O_2}^0 = p_{O_2}^l \quad (12)$$

where $p_{O_2}^l$ is the oxygen partial pressure at the anode.

2.3. Energy conservation equation

The voltage output for the SOFC with a pure ionic conduction electrolyte can be obtained as [26]:

$$V = E_{Th} - \eta_{act} - \eta_{ohm} - \eta_{conc} \quad (13)$$

where E_{Th} is theoretical reversible voltage of the fuel cell, η_{act} is activation overpotential, η_{ohm} is the ohmic overpotential and η_{conc} is the concentration overpotential. Taking the power inputs, outputs and all the energy losses into consideration and using Eq. (13), the energy conservation equation can be obtained as:

$$j_{O^{2-}} E_{Th} = j_{O^{2-}} \times \left(\frac{RT}{4F} \ln \frac{p_{O_2}^{ll}}{p_{O_2}^0} \right) \\ = j_L \cdot V + j_{O^{2-}} \cdot \eta_c + j_{O^{2-}} \cdot \eta_{ohm}^{O^{2-}} + |j_e| \cdot \eta_{ohm}^e, \quad (14)$$

where $\eta_{ohm}^{O^{2-}}$ is the ohmic loss for the ion transport and η_{ohm}^e is the ohmic loss for the electron transport. The concentration losses and ohmic losses in the electrodes are neglected in this model since these losses are very small under normal SOFC operating conditions.

According to Eq. (4), the ohmic loss for oxygen ion transport in the electrolyte is obtained as:

$$\eta_{ohm}^{O^{2-}} = \Delta\phi. \quad (15)$$

The ohmic loss for electron transport can be obtained by the Joule's law as:

$$|j_e| \cdot \eta_{ohm}^e = j_e \int_0^L \frac{j_e}{\sigma_e(x)} dx. \quad (16)$$

By substituting Eqs. (5) and (9) into Eq. (16) and integrating it, the ohmic loss for the electronic current is obtained as (the details are shown in Appendix),

$$\eta_{ohm}^e = \frac{RT}{4F} \ln \frac{p_{O_2}^L}{p_{O_2}^0} + \Delta\phi. \quad (17)$$

According to the Kirchhoff's law, the relationship between the load current density and the ionic and electronic current densities is given as:

$$j_L = j_{O^{2-}} + j_e \quad (18)$$

Substituting Eqs. (11), (15), (17) and (18) into Eq. (14), a supplementary condition for the oxygen partial pressure is obtained as:

$$\frac{RT}{4F} \ln \frac{p_{O_2}^L}{p_{O_2}^0} = V - \Delta\phi \quad (19)$$

2.4. Open-circuit voltage and leakage current density

The open circuit is an important operating condition for the SOFC with a MIEC electrolyte. Since the electronic current leakage at open circuit represents the worst case, the open-circuit voltage can be used to evaluate the performance of a MIEC electrolyte. Under open circuit the load current density is zero, thus:

$$j_L = j_{O^{2-}} + j_e = 0. \quad (20)$$

Substituting Eqs. (4) and (7) into Eq. (20),

$$\sigma_{O^{2-}} = -\frac{\sigma_e^0}{M_0} \left[M_0 \left(p_{O_2}^0 \right)^{-1/4} - \left(p_{O_2}^L \right)^{-1/4} \right]. \quad (21)$$

Combining Eqs. (4) and (19), the relationship of the open-circuit voltage and leakage current density (denoted by the ionic current density) is obtained as,

$$\exp \left[\frac{F}{RT} \frac{j_{O^{2-}}}{\sigma_{O^{2-}}} L \right] = \frac{\sigma_e^0}{\sigma_{O^{2-}}} \left(p_{O_2}^0 \right)^{-1/4} \left[1 - \exp \left(-\frac{F}{RT} V_{oc} \right) \right] + 1. \quad (22)$$

Eqs. (4) and (8)–(10) and (19) above form the system of equations for the polarization mathematical model for a SOFC with a MIEC electrolyte.

3. Comparison with experimental data

The experimental fuel cell uses samaria-doped ceria (SDC, $Sm_{0.2}Ce_{0.8}O_{3-\delta}$) as the electrolyte, 25 wt.% NiO + 75 wt.% SDC as the anode and 25 wt.% SDC + 65 wt.% $Sm_{0.5}Sr_{0.5}CoO_{3-\delta}$ (SSC) as the cathode.

3.1. Experimental procedures

The $Sm_{0.2}Ce_{0.8}O_{3-\delta}$ (SDC) and $Sm_{0.5}Sr_{0.5}CoO_{3-\delta}$ (SSC) are synthesized by the citrate–nitrate process. The composite anode and cathode are mixed respectively with an appropriate amount of terpineol with 6 wt.% ethyl cellulose to form pastes. The supported electrolyte is formed by dry-pressing method to a pellet (20 mm in diameter) with a 300 MPa pressure, and the anode paste is spread on the pellet to form a circular electrode (diameter: 10 mm, area: 0.785 cm^2). Then the anode and electrolyte are co-sintered for 4 h at 1200°C . The cathode paste is spread on the other side of the pellet to form the cathode, and a silver lead is adhered to the fuel cell pellet by silver paste. The fuel cell is sintered for 3 h at 1050°C . The finished fuel cell pellet is shown in Fig. 2a. During all the experiments, 40 sccm 3% humidified hydrogen (controlled by mass flow controller Sevenstar® CS200, Beijing Sevenstar Electronics Co.

Ltd.) was supplied to the anode and the cathode is open to the ambient air.

To measure the conductivity of the SDC, SDC is dry-pressed into a pellet with a diameter of 11.4 mm and thickness of 1.5 mm, and sintered for 4 h at 1200 °C. Silver paste is spread onto both sides of the SDC pellet as electrodes as showing in Fig. 2b. Two silver leads are adhered to each side of the SDC pellet to form the four-electrode arrangement in order to eliminate the lead resistance and contact resistance. The conductivity of the SDC is measured by the electrochemical impedance spectroscopy (EIS) method (HCP-803, Biologic SAS). First, the conductivity of the SDC pallet is measured in the ambient air environment to obtain the ionic conductivity of SDC since its electronic conductivity is negligible under such a condition. Then the total conductivity of the SDC pellet is measured in 3% humidified hydrogen at a flow rate of 40 sccm. Assuming the ionic conductivity is the same in both cases, the electronic temperature-dependent coefficient is determined by Eq. (24),

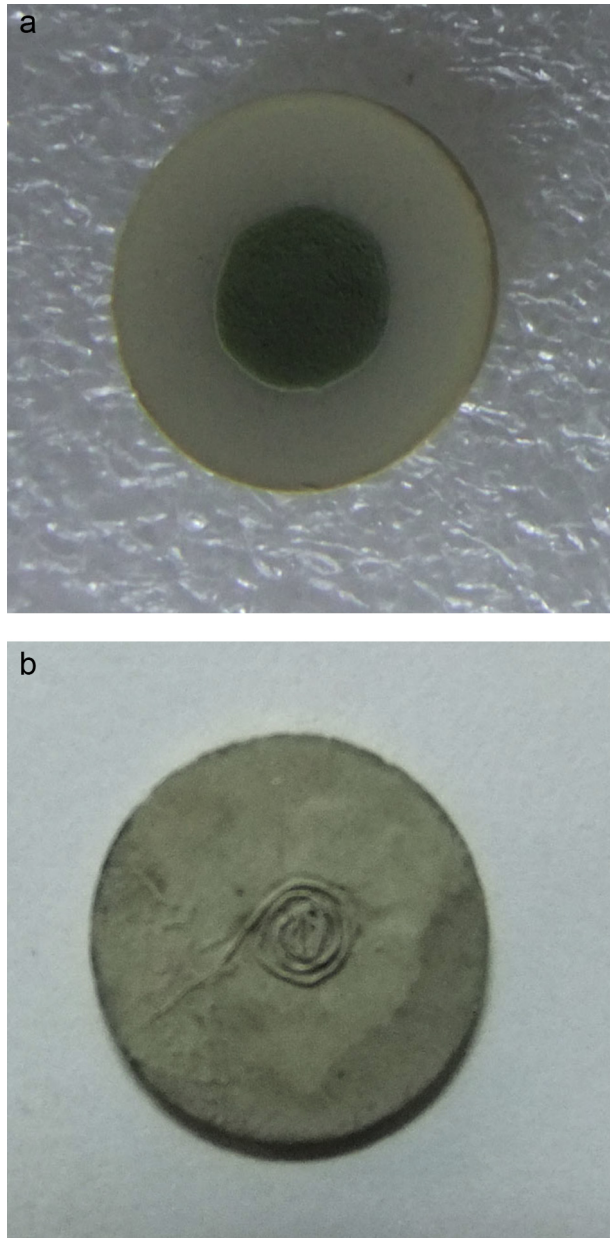


Fig. 2. The experimental (a) SOFC and (b) SDC pellet.

Table 1
Measured SDC conductivities at different temperatures.

Temperature/°C	700	600	500
Ionic conductivity/S cm ⁻¹	0.0332	0.0112	0.0037
Coefficient of electronic conductivity/S cm ⁻¹	2.77E-07	1.96E-08	6.15E-10

$$\sigma_t = \sigma_{O^{2-}} + \sigma_e = \sigma_{O^{2-}} + \sigma_e^0 p_{O_2}^{-1/4} \quad (24)$$

3.2. Comparison of model results with experimental data

The SDC conductivities determined by experiment are listed in Table 1. All the values are the average of three repeated tests.

In the model, the exchange current density is determined using Eqs. (10) and (22) from the measured open-circuit voltage, the oxygen partial pressure at the anode is obtained by the local equilibrium of the water vapor,

$$K_{an} = \frac{p_{H_2O}^l}{p_{H_2}^l \sqrt{p_{O_2}^l}} \quad (25)$$

The modeling results of polarization curves at three different temperatures of 500 °C, 600 °C and 700 °C are compared with the experimental data and are shown in Fig. 3. The modeling results agree reasonably well with the experimental data and the best agreement is obtained at 600 °C.

Fig. 4 shows the comparison of the modeling results with the experiment data for two electrolyte thicknesses at 600 °C and 700 °C, respectively. The comparison shows that the modeling results agree well with the experiment data for both electrolyte thicknesses. Both the modeling results and the experimental data show that the performance of SOFCs increases with the decrease in electrolyte thickness.

4. Parametric analysis of a SOFC with a MIEC electrolyte

The characteristics of a SOFC with a MIEC electrolyte are studied by analyzing the effects of some key parameters, including the electrolyte conductivities, electrolyte thickness and the cathode exchange current density.

4.1. Effect of electrolyte conductivity

Fig. 5 shows the dependence of the open-circuit voltage and leakage current density on the ionic conductivity at 600 °C. As shown in the figure, the open-circuit voltage of the SOFC with a MIEC electrolyte slightly increases with the increase of the electrolyte ionic conductivity, and the leakage current density increases approximately linearly with the ionic conductivity. Fig. 6 shows the dependence of the open-circuit voltage and leakage current density on the electronic temperature-dependent coefficient at 600 °C. As shown in the figure, in a realistic open-circuit potential range (e.g. >0.75 V) the open-circuit voltage decreases sharply while the leakage current density increases sharply with the increase of electrolyte electronic conductivity.

4.2. The effect of electrolyte thickness

Fig. 7 shows the effects of electrolyte thickness on the open-circuit voltage and leakage current density at 600 °C. The open-circuit voltage increases with the increase of the electrolyte thickness, and rate of increase decreases as the thickness of the electrolyte increases. The leakage current density decreases sharply

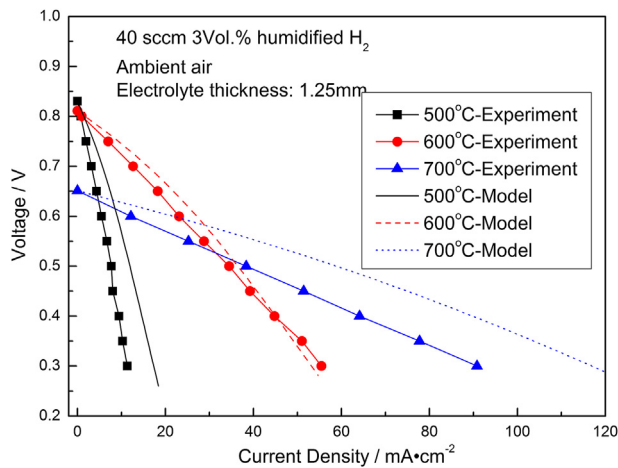


Fig. 3. Comparison of modeling results with experimental data at different temperatures.

when the electrolyte is very thin and the rate of decrease reduces very quickly as the electrolyte thickness increases.

The polarization and power density curves for different electrolyte thicknesses at 600 °C are shown in Fig. 8. With the increase of the electrolyte thickness the performance of the SOFC exhibits

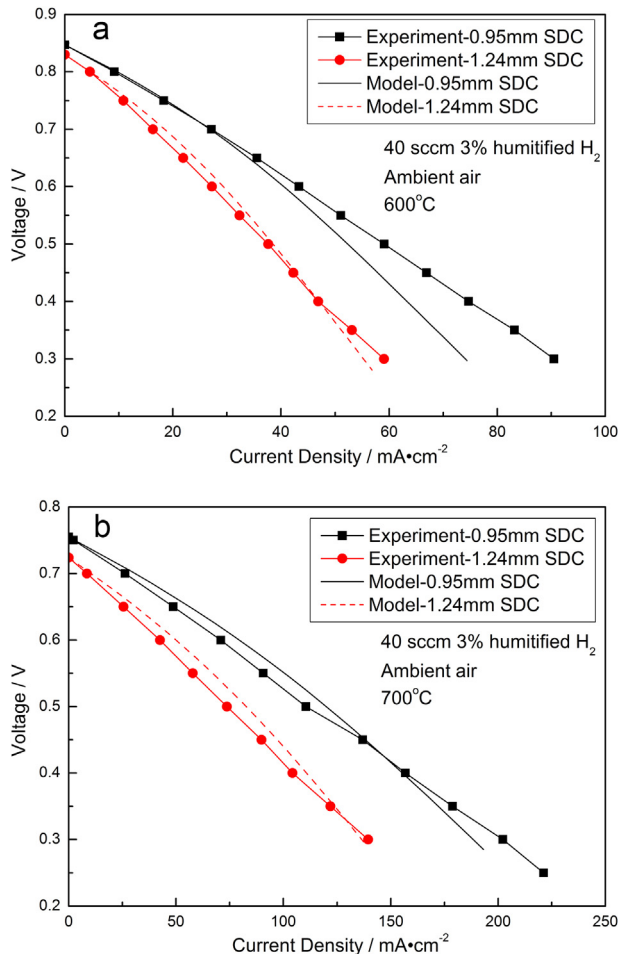


Fig. 4. Comparison of modeling results with experimental data at different electrolyte thicknesses and different operating temperatures (a. 600 °C, b. 700 °C).

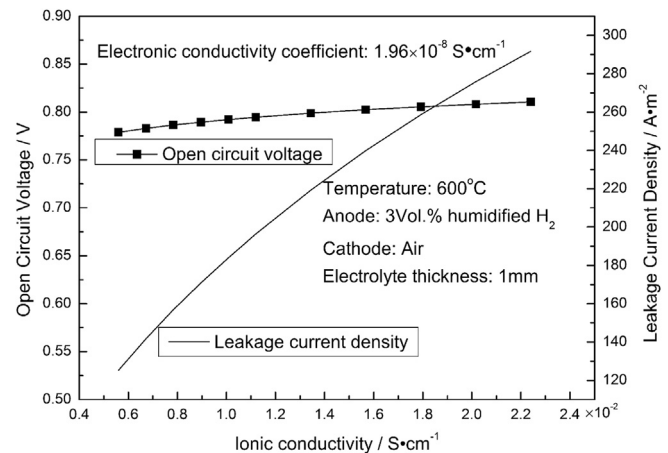


Fig. 5. The dependence of the open-circuit voltage and leakage current density on the ionic conductivity at 600 °C.

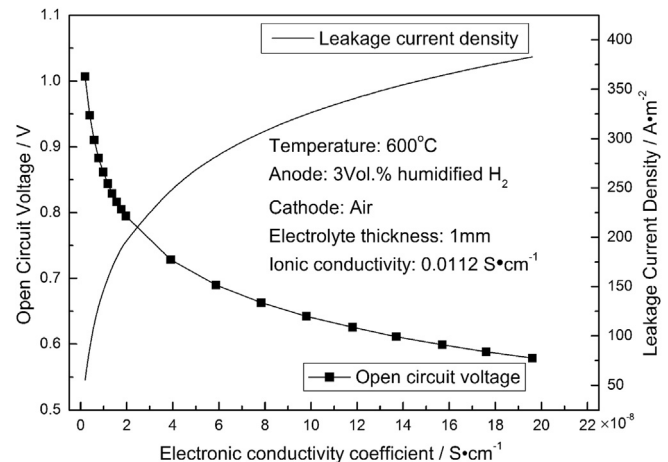


Fig. 6. The dependence of the open-circuit voltage and leakage current density on the electronic temperature-dependent coefficient at 600 °C.

significant decrease, and the performance reduction is not as significant when the electrolyte thickness is greater than 800 μ m. However the performance for the SOFC with a thinner electrolyte is

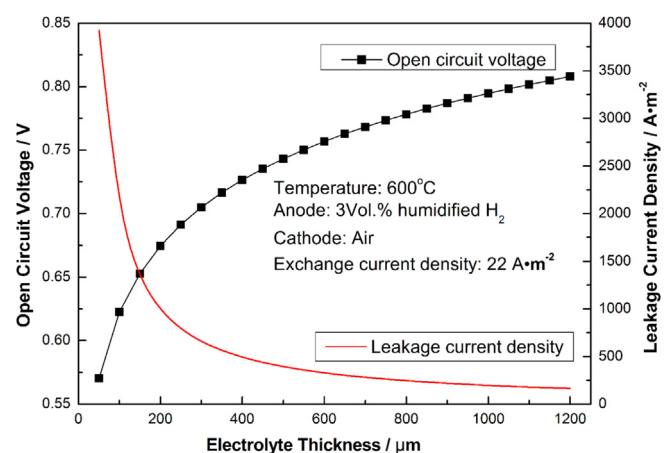


Fig. 7. The dependence of the open circuit voltage and leakage current density on the electrolyte thickness at 600 °C.

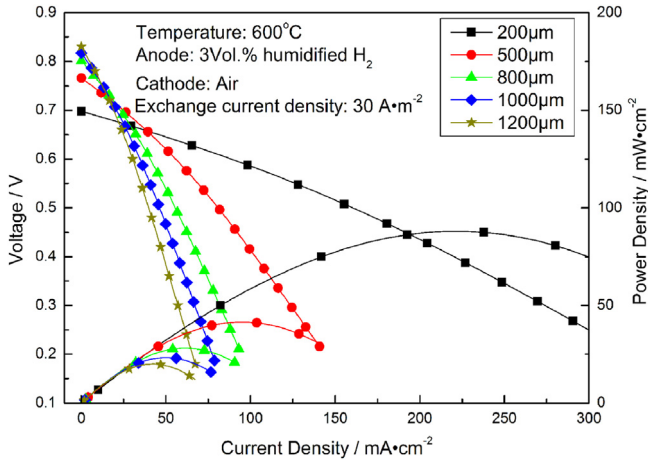


Fig. 8. The polarization curves and power density curves for different electrolyte thicknesses at 600 °C.

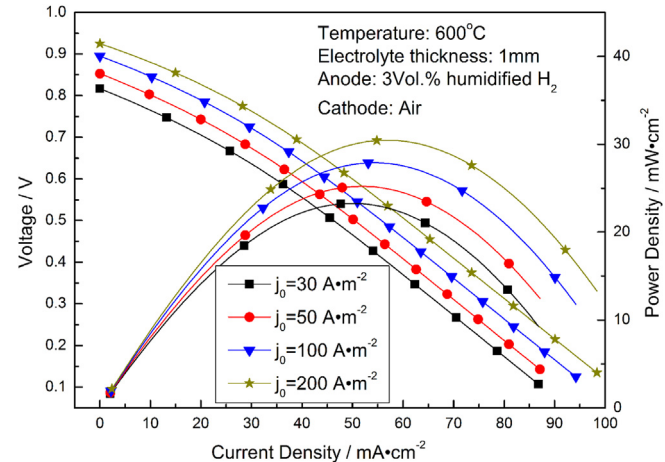


Fig. 11. The polarization curves and power density curves with different cathode exchange current densities at 600 °C.

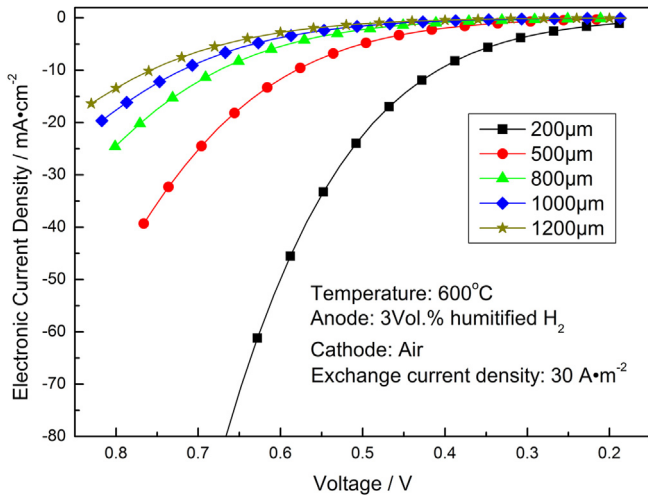


Fig. 9. The variations of the electronic current density with the operating voltage at 600 °C.

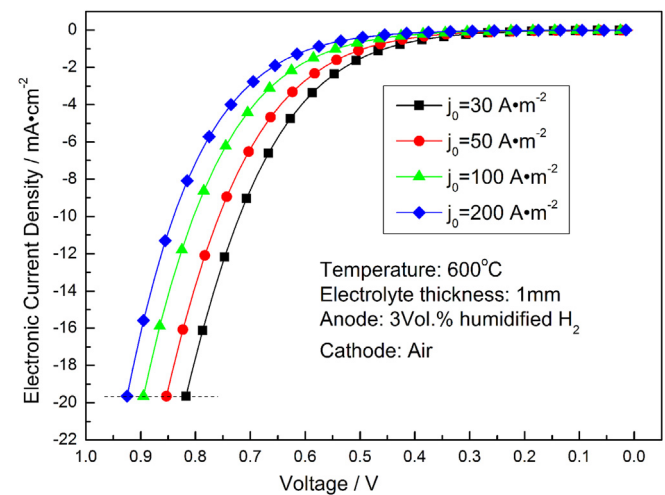


Fig. 12. The variations of the electronic current density with the operating voltage at 600 °C.

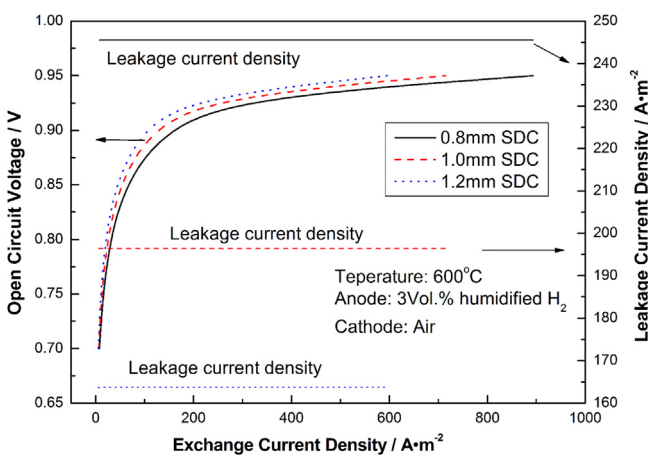


Fig. 10. The dependence of the open-circuit voltage and leakage current density on the cathode exchange current density at 600 °C.

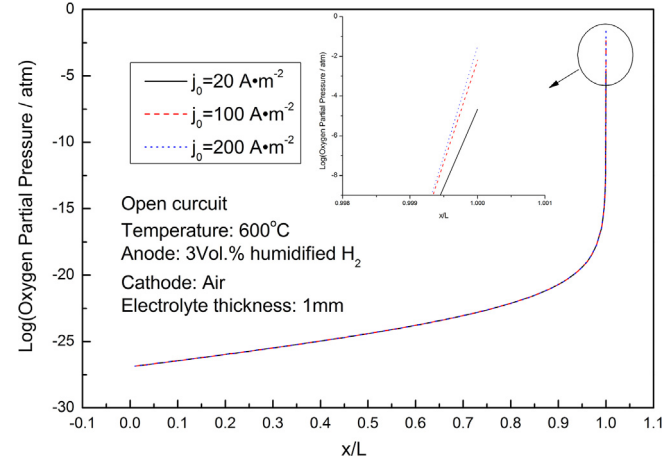


Fig. 13. The distribution of oxygen partial pressure in the electrolyte under open circuit for different cathode exchange current densities at 600 °C.

lower than that for a thicker electrolyte near the open-circuit voltage, where the leakage current is very high.

Fig. 9 shows the variations of the electronic current density with the operating cell voltage at 600 °C for different electrolyte thicknesses. The electronic current density decreases with the decrease of the operating voltage, and when the operating voltage is lower than a certain value the electronic current density approaches zero. At the same operating voltage, the electronic current density decreases with the increase of the electrolyte thickness.

In summary, the performance of a SOFC with a MIEC electrolyte is significantly affected by the MIEC thickness. As the MIEC thickness increases, the open-circuit voltage increases and the leakage current density decreases, but both current density and power density at a given operating voltage decrease. This is also true for the maximum power density. Thus the MIEC thickness must be optimized to achieve the desired optimal performance.

4.3. The effect of the cathode exchange current density

According to the Butler–Volmer equation (Eq. (10)), the exchange current density represents the electrode performance, thus the cathode exchange current density is taken as the parameter to study the effect of the cathode performance on the output characteristic of a SOFC with a MIEC electrolyte. The modeling results are shown in Figs. 10–13.

Fig. 10 shows the dependence of the open-circuit voltage and leakage current density on the cathode exchange current density at 600 °C. The open-circuit voltage initially rises rapidly as the exchange current density increases, and then the rate of increase decreases and curves become almost flat when the exchange current density is greater than about 200 A m⁻². It is interesting to note from Fig. 10 that the leakage current at the open circuit is constant, i.e. it is independent of the cathode exchange current density. This result appears to contradict with Eq. (22), which shows that the leakage current density depends on the open-circuit voltage. The reason for this seemingly contradiction is that the effect of the open-circuit voltage on the leakage current density is very slight under typical SOFC operating condition (0.6 < V_{OC} < 1.1 and T < 1073), since,

$$\exp\left(-\frac{F}{RT}V_{OC}\right) \ll 1.$$

Actually the leakage current density at open circuit can be expressed as,

$$j_{0^{2-}} \approx \frac{RT}{F} \frac{\sigma_{O^{2-}}}{L} \ln \left[\frac{\sigma_e^0}{\sigma_{O^{2-}}} (p_{O_2}^0)^{-1/4} + 1 \right] \quad (26)$$

Obviously, the leakage current density is dependent on the conductivities of the electrolyte, the electrolyte thickness and the anode oxygen partial pressure.

The polarization curves and power density curves with different cathode exchange current density at 600 °C are shown in Fig. 11. Both current density and power density increase with the increase of the cathode exchange current density. It is interesting to note from Fig. 11 that the I–V curves shift upward as the cathode exchange current density increases, but the shape of the polarization curves remains unchanged.

Fig. 12 shows the results of the variations of electronic current density with the cell operating voltage at different cathode exchange current densities at 600 °C. At a specific operating voltage, the electronic current density decreases with the increase of the cathode exchange current density. However the maximum electronic current densities for all the different cathode exchange

current densities are the same, which is consistent with the results shown in Fig. 10.

The distributions of oxygen partial pressure in the electrolyte under open circuit for different cathode exchange current densities at 600 °C are shown in Fig. 13. The oxygen partial pressure increases linearly with x, the distance from the anode, from x = 0 until x/L is greater than 0.95, where it increases very rapidly. The distribution of oxygen partial pressure is mostly independent of the cathode exchange current density, except near the cathode side (x/L ≥ 0.95), where the oxygen partial pressure increases slightly with increase of the cathode exchange current density. On the cathode surface, x = L, the oxygen partial pressure increases slightly with the increase of cathode exchange current density.

4.4. The distribution of oxygen partial pressure

The distributions of oxygen partial pressure in the electrolyte for different operating voltages at 600 °C are shown in Fig. 14. Same as at open circuit, the oxygen partial pressure at all cell voltages increases linearly with the distance from anode side, and when x/L is greater than about 0.95 it increase rapidly. As the cell operating voltage decreases, the oxygen partial pressure increases. The oxygen partial pressure is the lowest at open circuit.

5. Conclusion

A polarization model for a solid oxide fuel cell with a MIEC electrolyte is developed based on the charge transport equation and the energy conservation equation is included as an additional condition to complete the model. The modeling results are first compared with the experimental data obtained in the lab, and good agreements are obtained. Then the model is used to study the effects of various key parameters, including the conductivities of the MIEC, the electrolyte thickness and the cathode exchange current density. The model is also used to obtain the distribution of oxygen partial pressure in the electrolyte at different operating voltages. The following conclusions may be obtained from the modeling results:

- 1) The leakage current density increases almost linearly with electrolyte ionic conductivity, while the open-circuit voltage is not significantly affected.

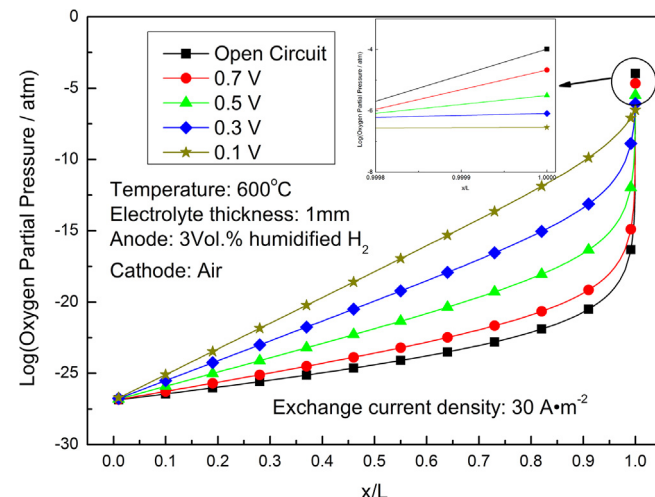


Fig. 14. The distribution of oxygen partial pressure in the electrolyte for different operating voltages at 600 °C.

- 2) The leakage current density increases sharply and the open-circuit voltage decreases sharply with the electrolyte electronic conductivity.
- 3) The open-circuit voltage increases with electrolyte thickness, while the power density decreases with electrolyte thickness. Thus the electrolyte thickness should be optimized depending on the desired operating voltage and other operating conditions.
- 4) The cathode exchange current density has almost no effect on the leakage current density; however the open-circuit voltage and fuel cell performance increase significantly with cathode exchange current density.
- 5) The oxygen partial pressure in the electrolyte increases with the decrease in operating voltage.

Acknowledgments

This work was supported by the NSFC Fund for Creative Research Groups (Grant No. 51121092).

Nomenclature

A	active surface area, cm^{-2}
c_i	concentration of species i , mol m^{-3}
D_i	diffusivity of species i , $\text{m}^2 \text{s}^{-1}$
e	elementary charge, $1.60218 \times 10^{-19} \text{ C}$
E_{Th}	theoretical reversible voltage of fuel cell
F	Faraday constant, 96485 C mol^{-1}
I	current flowing through the load, A
J_i	mole flux of the charge i
j_L	total current density defined by $j_L = I/A$, A cm^{-2}
j_i	current density of charge i , A cm^{-2}
K	equilibrium coefficient
L	thickness of the electrolyte, m
p_i	partial pressure of species i , bar
P	power density, W cm^{-2}
R	ideal gas constant, $8.314 \text{ J (K mol)}^{-1}$
T	absolute temperature, K
V	cell voltage, V
V_{oc}	open-circuit voltage, V
$V_{\text{rev},c}$	theoretical reversible voltage in the cathode, V
x	position variable, m
z_i	valence of charge i ,

Greek symbol

α_c	cathode transfer coefficient, 0.5
η_i	polarization loss, V
σ	conductivity, S m^{-1}
ϕ	inner electric potential, V
μ_i	chemical potential of species i , J mol^{-1}

Superscripts

0	the boundary of electrolyte at the anode
L	the boundary of electrolyte at the cathode
I	parameters in anode
II	parameters in cathode
ref	parameters for reference
O^{2-}	oxygen ion
e	electron

Subscripts

O_2	oxygen
O^{2-}	oxygen ion
e	electron
c	cathode
an	anode
act	activation of electrode reaction

ohm ohmic
conc concentration

Abbreviation

ADC	acceptor-doped ceria
EIS	electrochemical impedance spectroscopy
MIEC	mixed ionic and electronic conductor
SDC	samarium doped ceria
SOFC	solid oxide fuel cell
SSC	cathode material $\text{Sm}_{0.5}\text{Sr}_{0.5}\text{CoO}_3-\delta$
YSZ	yttria stabilized zirconia

Appendix

The ohmic loss of electron transport in the MIEC

According to the Joule's law shown in Eq. (16), the ohmic loss of electron transport in the MIEC can be calculated by:

$$\eta_{\text{ohm}}^e = -j_e \int_0^L \frac{dx}{\sigma_e(x)}. \quad (\text{A-1})$$

Substituting the electronic conductivity by Eq. (5), the ohmic loss becomes,

$$\eta_{\text{ohm}}^e = -\frac{j_e}{\sigma_e^0} \int_0^L \frac{dx}{[p_{O_2}(x)]^{-1/4}}. \quad (\text{A-2})$$

According to Eq. (9), the ohmic loss can be written as,

$$\eta_{\text{ohm}}^e = -\frac{j_e}{\sigma_e^0} \int_0^L \frac{dx}{(p_{O_2}^0)^{-1/4} \exp\left(-\frac{F}{RT} \frac{j_{O^{2-}}}{\sigma_{O^{2-}}} x\right) - \frac{j_e \sigma_{O^{2-}}}{j_{O^{2-}} \sigma_e^0} \left[\exp\left(-\frac{F}{RT} \frac{j_{O^{2-}}}{\sigma_{O^{2-}}} x\right) - 1 \right]}. \quad (\text{A-3})$$

Rearranging Eq. (A-3), we have,

$$\eta_{\text{ohm}}^e = -\frac{j_e}{\sigma_e^0} \int_0^L \frac{\exp\left(\frac{F}{RT} \frac{j_{O^{2-}}}{\sigma_{O^{2-}}} x\right) dx}{(p_{O_2}^0)^{-1/4} - \frac{j_e \sigma_{O^{2-}}}{j_{O^{2-}} \sigma_e^0} + \frac{j_e \sigma_{O^{2-}}}{j_{O^{2-}} \sigma_e^0} \exp\left(\frac{F}{RT} \frac{j_{O^{2-}}}{\sigma_{O^{2-}}} x\right)}. \quad (\text{A-4})$$

Integrating Eq. (A-4) from $x = 0$ to $x = L$, the ohmic loss is obtained as,

$$\eta_{\text{ohm}}^e = -\frac{RT}{F} \ln \frac{(p_{O_2}^0)^{-1/4} - \frac{j_e \sigma_{O^{2-}}}{j_{O^{2-}} \sigma_e^0} + \frac{j_e \sigma_{O^{2-}}}{j_{O^{2-}} \sigma_e^0} \exp\left(\frac{F}{RT} \frac{j_{O^{2-}}}{\sigma_{O^{2-}}} L\right)}{(p_{O_2}^0)^{-1/4}}. \quad (\text{A-5})$$

According to Eq. (9), the oxygen partial pressure at $x = L$ can be obtained as,

$$(p_{O_2}^L)^{-1/4} = (p_{O_2}^0)^{-1/4} \exp\left(-\frac{F}{RT} \frac{j_{O^{2-}}}{\sigma_{O^{2-}}} L\right) - \frac{j_e \sigma_{O^{2-}}}{j_{O^{2-}} \sigma_e^0} \left[\exp\left(-\frac{F}{RT} \frac{j_{O^{2-}}}{\sigma_{O^{2-}}} L\right) - 1 \right]. \quad (\text{A-6})$$

Substituting Eq. (A-6) into Eq. (A-5), the ohmic loss can be shown to be,

$$\eta_{\text{ohm}}^{\text{e}} = -\frac{RT}{F} \ln \frac{(p_{\text{O}_2}^L)^{-1/4} \exp\left(\frac{F}{RT} \frac{j_{\text{O}_2^-}}{\sigma_{\text{O}_2^-}} L\right)}{(p_{\text{O}_2}^0)^{-1/4}}. \quad (\text{A-7})$$

Rearranging Eq.(A-7), we obtain

$$\eta_{\text{ohm}}^{\text{e}} = \frac{RT}{4F} \ln \frac{p_{\text{O}_2}^L}{p_{\text{O}_2}^0} - \frac{j_{\text{O}_2^-}}{\sigma_{\text{O}_2^-}} L \quad (\text{A-8})$$

From Eq. (4), the expression of ohmic loss can be written as,

$$\eta_{\text{ohm}}^{\text{e}} = \frac{RT}{4F} \ln \frac{p_{\text{O}_2}^L}{p_{\text{O}_2}^0} + \Delta\phi \quad (\text{A-9})$$

References

- [1] A.S. Nesaraj, J. Sci. Ind. Res. 69 (2010) 169–176.
- [2] O. Yamamoto, Electrochim. Acta 45 (2000) 2423–2435.
- [3] H. Inaba, H. Tagawa, Solid State Ionics 83 (1996) 1–16.
- [4] B. Dalslet, P. Blennow, P. Hendriksen, N. Bonanos, D. Lybye, M. Mogensen, J. Solid State Electrochem. 10 (2006) 547–561.
- [5] S.C. Singhal, K. Kendall, High-temperature Solid Oxide Fuel Cells: Fundamentals, Design and Applications, Elsevier, Oxford, 2003.
- [6] M. Mori, Y. Liu, S. Hashimoto, K. Takei, Electrochemistry 77 (2009) 178–183.
- [7] T. Matsui, T. Kosaka, M. Inaba, A. Mineshige, Z. Ogumi, Solid State Ionics 176 (2005) 663–668.
- [8] M. Andersson, J. Yuan, B. Sundén, Appl. Energy 87 (2010) 1461–1476.
- [9] D. Bhattacharyya, R. Rengaswamy, Ind. Eng. Chem. Res. 48 (2009) 6068–6086.
- [10] C.O. Colpan, I. Dincer, F. Hamdullahpur, Int. J. Energy Res. 32 (2008) 336–355.
- [11] S. Kakac, A. Pramuanjaroenkit, X.Y. Zhou, Int. J. Hydrogen Energy 32 (2007) 761–786.
- [12] K. Wang, D. Hissel, M.C. Péra, N. Steiner, D. Marra, M. Sorrentino, C. Pianese, M. Monteverde, P. Cardone, J. Saarinen, Int. J. Hydrogen Energy 36 (2011) 7212–7228.
- [13] K.L. Duncan, K.-T. Lee, E.D. Wachsman, J. Power Sources 196 (2011) 2445–2451.
- [14] C. Daan, L. Qiang, C. Fanglin, J. Power Sources (2010) 4160–4167.
- [15] K.L. Duncan, E.D. Wachsman, J. Electrochem. Soc. 156 (2009) B1030–B1038.
- [16] M. Godickemeier, L.J. Gauckler, J. Electrochem. Soc. 145 (1998) 414–421.
- [17] I. Riess, M. Gödicke, L.J. Gauckler, Solid State Ionics 90 (1996) 91–104.
- [18] I. Riess, J. Electrochem. Soc. 128 (1981) 2077–2081.
- [19] D.S. Tannhauser, J. Electrochem. Soc. 125 (1978) 1277–1282.
- [20] N.S. Choudhury, J.W. Patterson, J. Electrochem. Soc. 118 (1971) 1398–1403.
- [21] R. Singh, K. Thomas Jacob, Int. J. Eng. Sci. 42 (2004) 1587–1602.
- [22] Z. Chen, J. Electrochem. Soc. 151 (2004) A1576–A1583.
- [23] S. Yuan, U. Pal, J. Electrochem. Soc. 143 (1996) 3214–3222.
- [24] J.W. Fergus, R. Hui, X. Li, D.P. Wilkinson, J. Zhang, Solid Oxide Fuel Cells: Materials Properties and Performance, CRC Press, New York, 2009.
- [25] S. Shen, L. Guo, H. Liu, Int. J. Hydrogen Energy 38 (2013) 1967–1975.
- [26] R. O’Hayre, S.-W. Cha, W. Colella, F.B. Pruzb, Fuel Cell Fundamentals, John Wiley & Sons, New York, 2005.